Flexible, TADF-Based Organic X-ray Scintillating Films for High-Resolution Imaging

Haoqiang Xu, Wenjing Zhao, Xinning Zhang, Jingjing Cui, Zhenhua Wang, Xiaowang Liu, Junqing Shi and Lei Ji**

Frontiers Science Center for Flexible Electronics (FSCFE), Shaanxi Institute of Flexible Electronics (SIFE) & Shaanxi Institute of Biomedical Materials and Engineering (SIBME), Northwestern Polytechnical University (NWPU), 127 West Youyi Road, Xi'an 710072, China.

Correspondence to: iamlji@nwpu.edu.cn; shi2013junqing@163.com

Methods

Chemicals: Carbazole (98%), 3,6-dichloro-9H-carbazole (98%), 3,6-dibromo-9H-carbazole (98%), 3,6-diiodo-9H-carbazole (98%), Potassium Tert-Butoxide (98%), Pentafluorobenzonitrile (98%), N, N-Dimethylformamide (SafeDry, with molecular sieves, Safeseal, 99.8%), Petroleum Ether (PE, ACS reagent), Ethyl Acetate (EA, ACS reagent), Dichloromethane (DCM, ACS reagent), Acetone (ACS reagent) were purchased from Adamas. BGO was purchased from Shanghai Lanjing Optoelectronic Technology Co., Ltd. All chemicals were used as received.

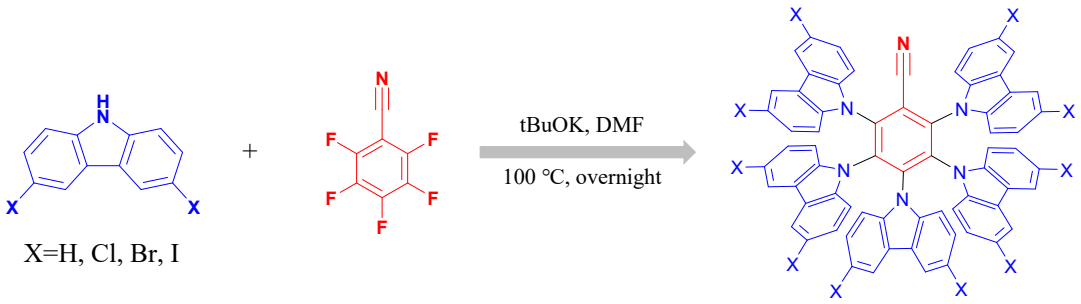

General synthesis methods: Different halogen substituted carbazoles (55 mmol) were dissolved in a 500 ml double-necked flask containing 150 ml of dry anhydrous DMF under argon atmosphere. Potassium tert-butoxide (60 mmol) was added and stirred at room temperature for 2.5 h. Pentafluorobenzonitrile (10 mmol) was added directly thereafter and the reaction was warmed up to 100 °C overnight. After completion of the reaction, it was poured into a beaker with 800 ml of ice water and the crude product was collected by filtration of the filter cake. H-CzBN and Cl-CzBN were purified using column chromatography to obtain the products (PE: DCM=10:1). Br-CzBN and I-CzBN were obtained by collecting the filter cake after pulping with the solvents DCM, acetone, and EA.

H-CzBN (yellow green solid, yield 81%). ^{1}H NMR (500 MHz, DMSO) δ 7.87 - 7.82 (m, 8H), 7.72 (dd, J = 15.2, 8.2 Hz, 6H), 7.38 (d, J = 7.6 Hz, 4H), 7.32 (d, J = 7.6 Hz, 2H), 7.13 (dd, J = 11.8, 4.7 Hz, 4H), 7.07 (t, J = 7.4 Hz, 4H), 6.76 - 6.63 (m, 10H), 6.58 (dd, J = 11.4, 4.2 Hz, 2H);

^{13}C NMR (125 MHz, DMSO) δ 143.04 141.60 139. 78 138.75 138.53 125.4 124.02 123.26 122.99 122. 93 121.04 120.48 120.39 119.56 119. 45 117.69 112.58 112.27 112.07

Cl-CzBN (green solid, yield 78%). ^{1}H NMR (500 MHz, DMSO) δ 8.14 (t, J = 7.9 Hz, 4H), 7.79 - 7.68 (m, 10H), 7.62 (d, J = 8.9 Hz, 2H), 7.57 (t, J = 7.3 Hz, 4H), 7.30 (dd, J = 8.8, 2.0 Hz, 4H), 6.88 (dd, J = 8.8, 1.9 Hz, 4H), 6.82 (dd, J = 8.8, 2.0 Hz, 2H).

^{13}C NMR (125 MHz, DMSO) δ 142.25141.19 139.18 138.4 137.93 137.42 137.29 126.6 126.52 126.44 125.92 125.84 125.22 123.89 123.54 121.25 120.79 120.56 113.23

Br-CzBN (green solid, yield 75%). ^{1}H NMR (500 MHz, DMSO) δ 8.30 (d, J = 1.8 Hz, 4H), 7.90 (d, J = 1.9 Hz, 4H), 7.85 (d, J = 1.8 Hz, 2H), 7.67 (d, J = 8.8 Hz, 4H), 7.57 (d, J = 8.8 Hz, 2H), 7.52 (d, J = 8.7 Hz, 4H), 7.41 (dd, J = 8.8, 1.9 Hz, 4H), 6.99 (dd, J = 8.8, 1.9 Hz, 4H), 6.94 (d, J = 10.5 Hz, 2H).

I-CzBN (green solid, yield 60%). ^{1}H NMR (500 MHz, DMSO) δ 8.40 (s, 4H), 7.99 (s, 4H), 7.94 (s, 2H), 7.52 (dd, J = 18.2, 8.7 Hz, 8H), 7.41 - 7.35 (m, 7H), 7.08 (d, J = 8.7 Hz, 4H), 7.02 (d, J = 9.5 Hz, 2H).

PMMA Film Preparation: Mixed 700 mg R-CzBN compound with 7 ml $CHCl_3$ and stirred at room temperature for 1 h to make them well dispersed. Then added 1000 mg

PMMA and stirred at room temperature for another 8 h. Poured the mixture into a special mold and sealed the mold with a porous sealing film to allow the solvent to evaporate completely. In this way, the scintillator films used for each test were obtained. By using this method, PMMA films with varied ratios of R-CzBN were prepared.

PDMS Film Preparation: Mixed 0.8 g I-CzBN with 10 ml $CHCl_3$ and then add a silicone elastomer kit (SYLGARD 184) by a weight ratio of 10:1. After stirring 6 hours and evacuate for 3 hours to remove air bubbles and volatile substances, the mixture was poured on a container and cured at 313 K for 24 h. The mass ratio between I-CzBN and PDMS was 1.5%. Finally, a 100 * 100 * 0.5 mm flexible film was obtained.

Characterization section:

^{1}H NMR spectra ware recorded at 25 ℃ on a Bruker Advance spectrometer (500 MHz) in $(CD_3)_2SO$. UV-visible absorption spectra were recorded on HITACHI UH5700 spectrometer. All fluorescence spectra were recorded on Edinburgh FLS1000 spectrometer with a Xe lamp as the excitation source for the stead-state measurements, and EPLED-380 diodes as the excitation source for the lifetime measurements. The PLQYs were measured by an integrated sphere (PYNECT, PN-PL100), with a Multiwavelength LEDs source (Qingdo Solar Scientific Instrument High-tech Co., LTD, UMW-MO-60A). The radioluminescence spectra by X-ray (SPRay, SPR50200HB) were recorded on an Ocean Optics spectrophotometer (QE65000).

The detection limit was calculated according to the literature[1].

X-ray attenuation ability:

The attenuation coefficient (AE, %) can be calculated through the following equation:

$$AE(\varepsilon,d) = \left(1 - e^{-c(\varepsilon)\rho d}\right) \times 100\%$$

where *c(ε)* is the photon cross section function obtained from the XCOM database of the National Institute of Standards and Technology, ρ and d are the density and thickness of the scintillator.

Light yield calculation: By integrating the X-ray-induced RL spectra and comparing the results with those found for the BGO reference, we obtained the relative light yield. A commercial BGO scintillators (20*20*0.1 mm; light yield, ~10000 photons MeV^{-1}) ware used as the reference to estimate the light yield of the PMMA film samples (20*20*0.1 mm). We just calculate real RL intensity as the image resolution and quality

were controlled by the RL intensity. **Figure S18** shows the equipment diagram. The specific calculation formula is as follows:

$$RLLY_{R-CzBN} = RLLY_{BGO} \times \frac{A_{R-CzBN}}{A_{BGO}}$$

$RLLY_{\text{R-CzBN}}$, the calculated light yields of R-CzBN; $RLLY_{\text{BGO}}$, the light yield of BGO; $A_{\text{R-CzBN}}$, the spectral integral area of R-CzBN; A_{BGO}, the spectral area of BGO. The $A_{\text{R-CzBN}}$ and A_{BGO} were calculated from Figure 3b.

X-ray imaging:

The X-ray imaging system was constructed as shown in Figure 4a. The high-resolution X-ray imaging was measured under an X-ray with Au target (60 kV, 200 μA). The imaging object is placed 5 cm away from the X-ray source and the radiation dose rate is 18.6 mGy s^{-1}. All the X-ray imaging photos were taken by a commercial camera (SONY Alpha 7R IV.). The ISO, aperture shutter and exposure time were set at 12800, F2.8 and 0.5 and 1 s.

Calculations:

DFT has been used to perform geometry optimizations of the studied molecules and the B3LYP functional and 6-31G(d) basis set with the Los Alamos basis set LanL2DZ were used to efficiently model the heavy atoms in the TADF molecules. The frequency calculation confirmed all the minima for the ground states. All the calculations were performed using Gaussian 16 packages [2].

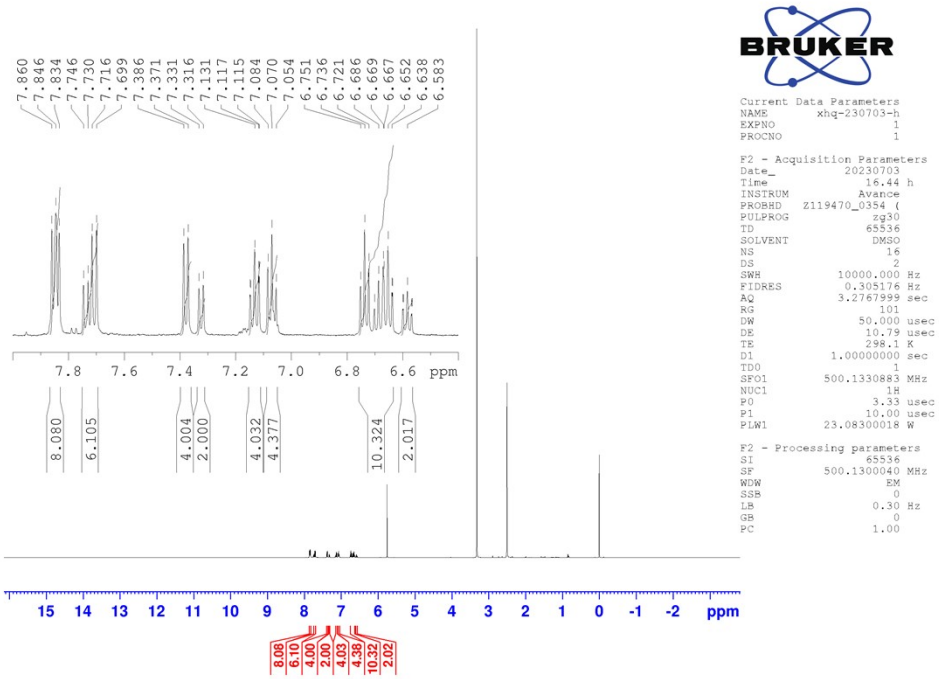

Figure S1 The ^{1}H NMR spectrum of H-CzBN molecule in $(CD_3)_2SO$.

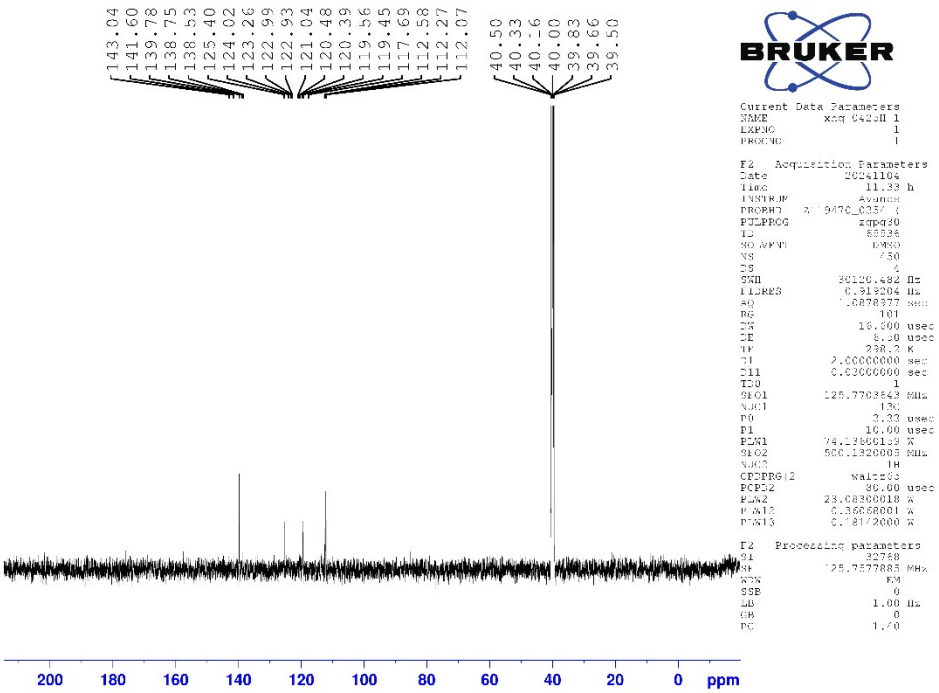

Figure S2 The ^{13}C NMR spectrum of H-CzBN molecule in $(CD_3)_2SO$

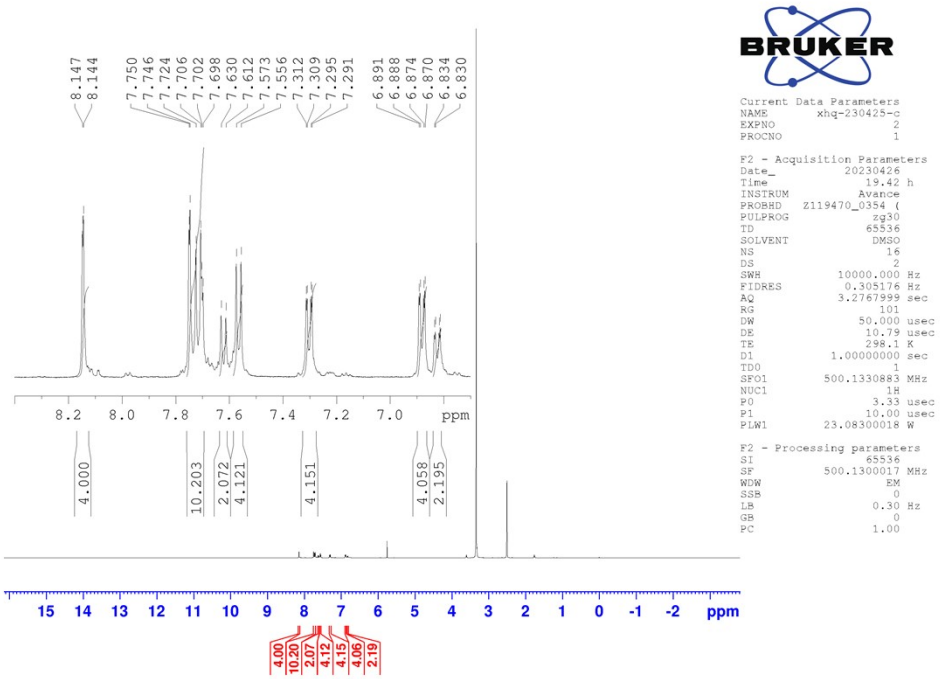

Figure S3 The ^{1}H NMR spectrum of Cl-CzBN molecule in $(CD_3)_2SO$.

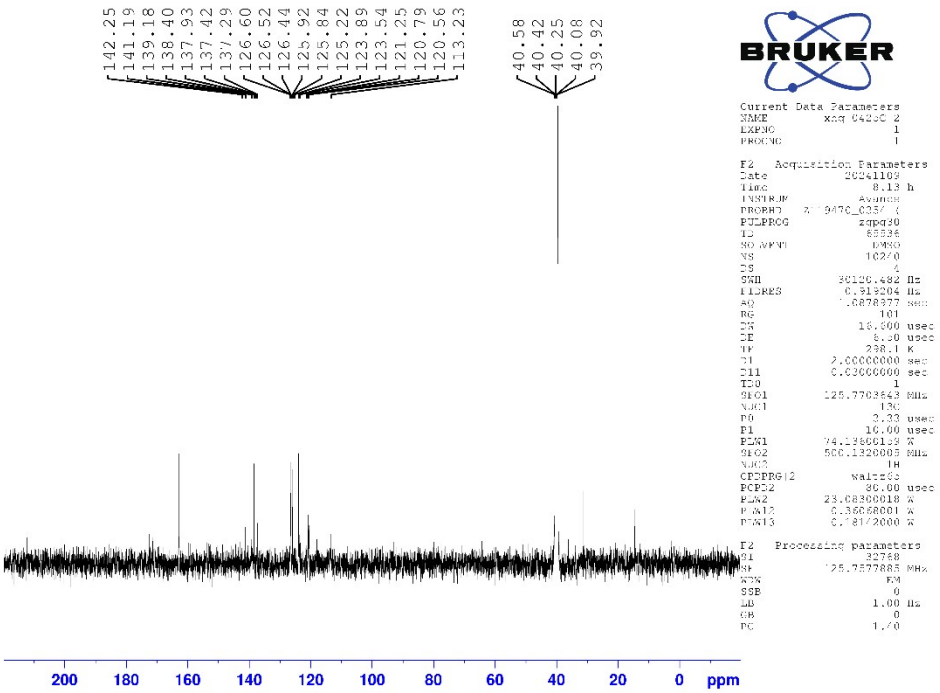

Figure S4 The ^{13}C NMR spectrum of Cl-CzBN molecule in $(CD_3)_2SO$.

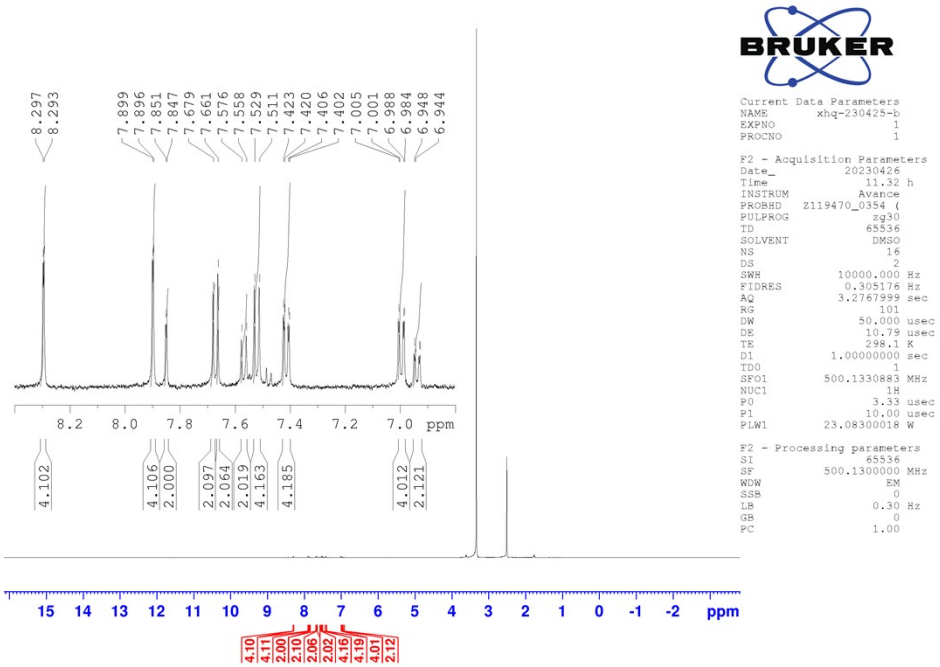

Figure S5 The ^{1}H NMR spectrum of Br-CzBN molecule in $(CD_3)_2SO$.

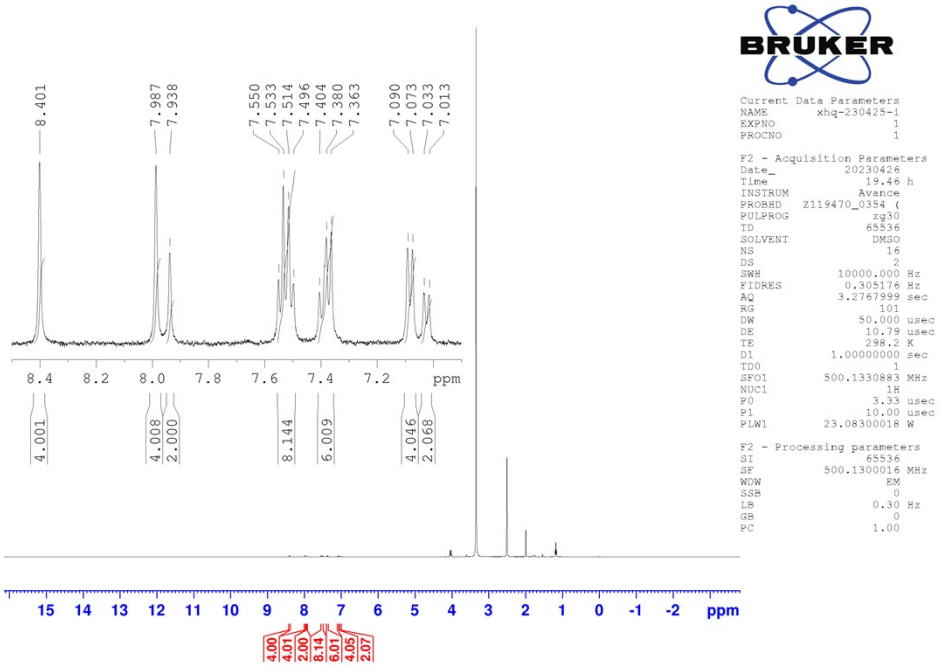

Figure S6 The ^{1}H NMR spectrum of I-CzBN molecule in $(CD_3)_2SO$.

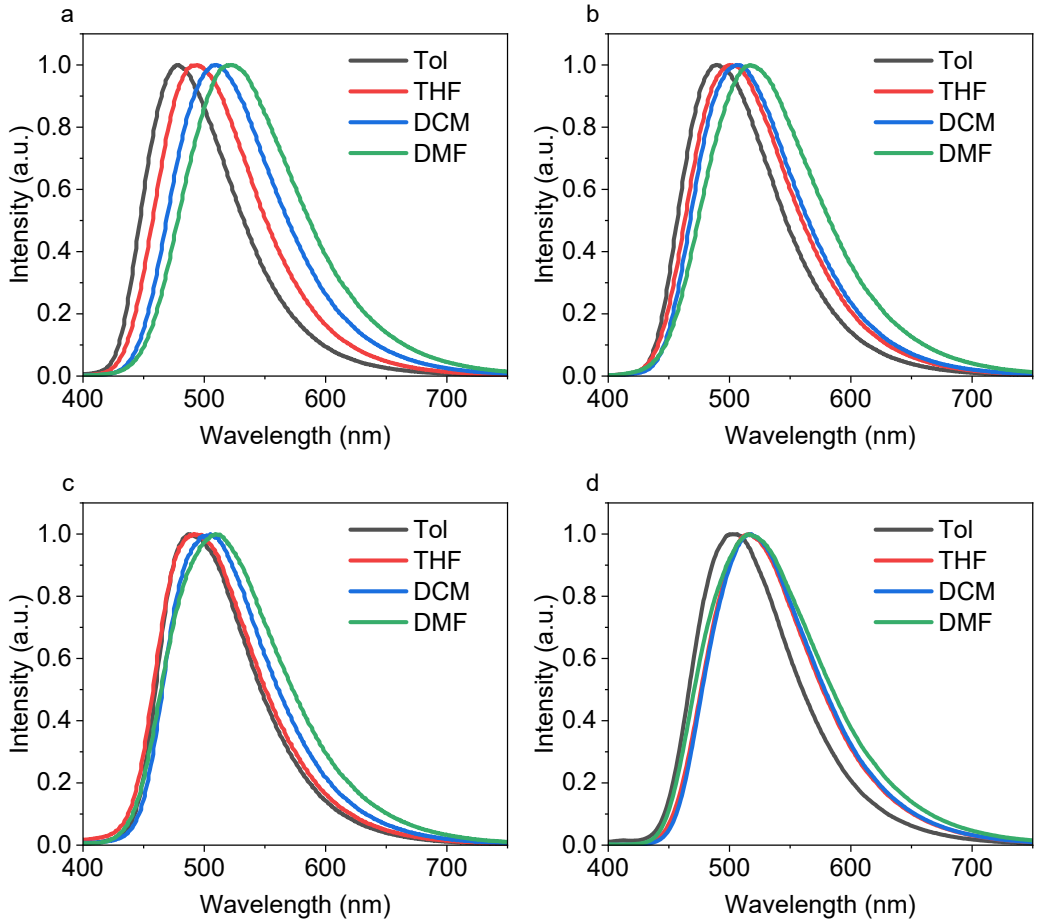

Figure S7 Solvent dependent PL spectra of (a) H-CzBN, (b) Cl-CzBN, (c) Br-CzBN, and (d) I-CzBN.

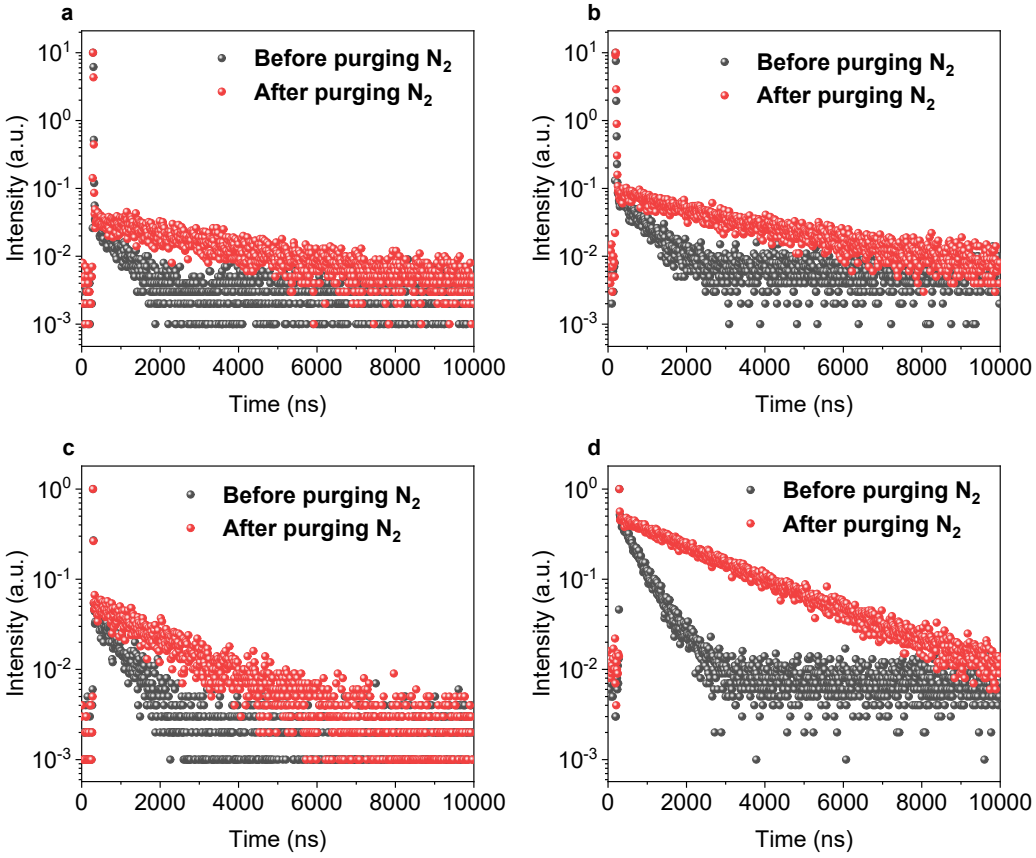

Figure S8 Transient PL decay profiles of (a) H-CzBN, (b) Cl-CzBN, (c) Br-CzBN, and (d) I-CzBN in toluene solution before (black) and after (red) purging nitrogen gas for 5 min.

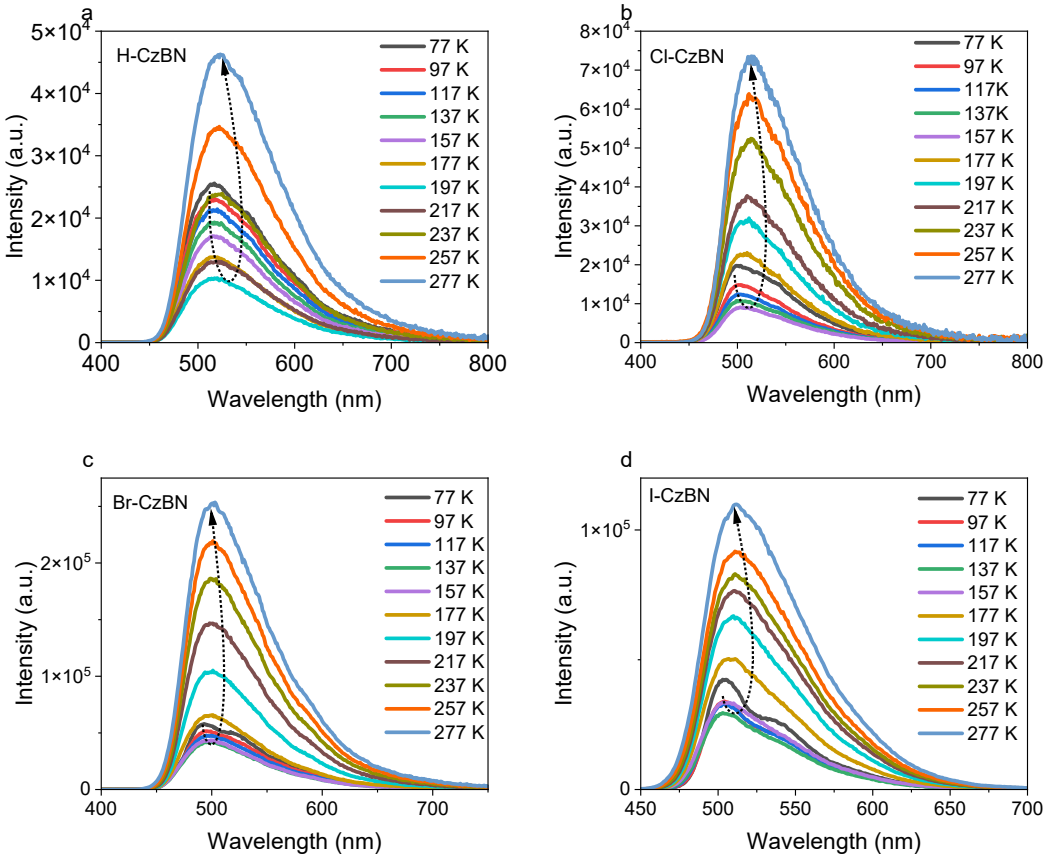

Figure S9 Temperature-dependent PL profiles of (a) H-CzBN, (b) Cl-CzBN, (c) Br-CzBN, and (d) I-CzBN in neat film.

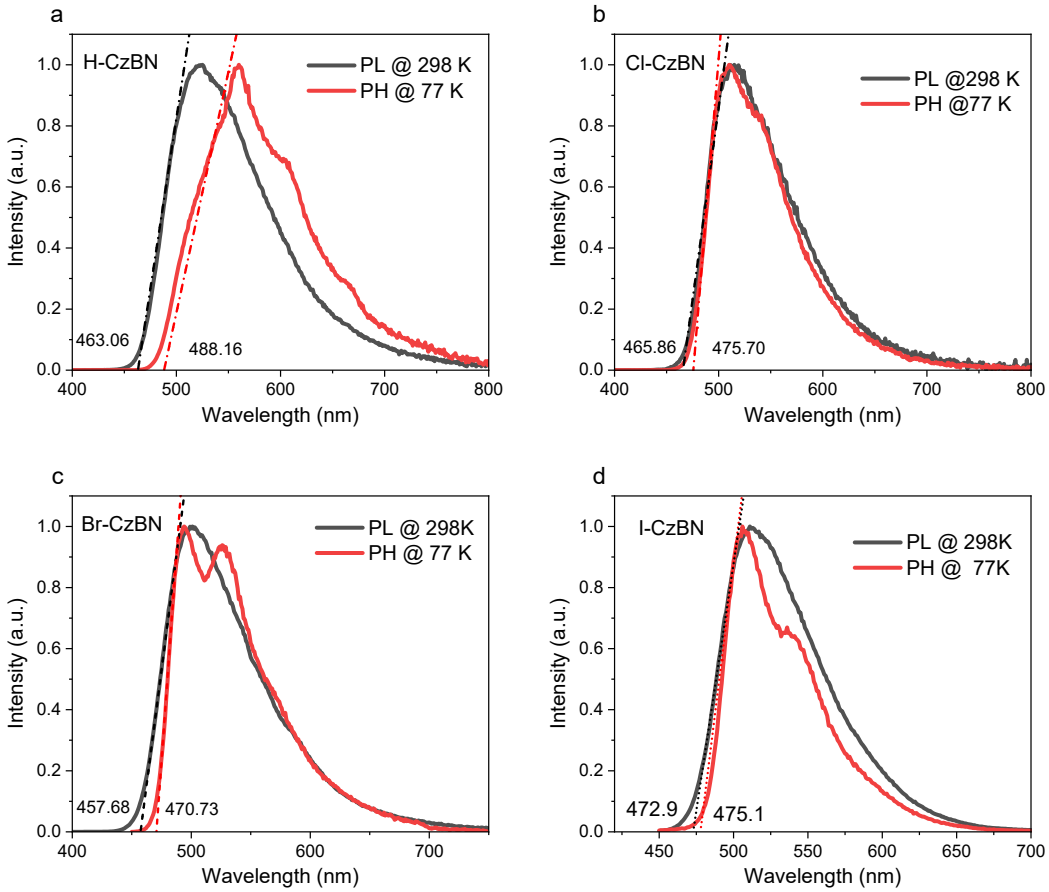

Figure S10 Normalized fluorescence (298 K) and phosphorescence (77 K) spectra of H-CzBN (a), Cl-CzBN (b), Br-CzBN (c), and I-CzBN (d) in neat film.

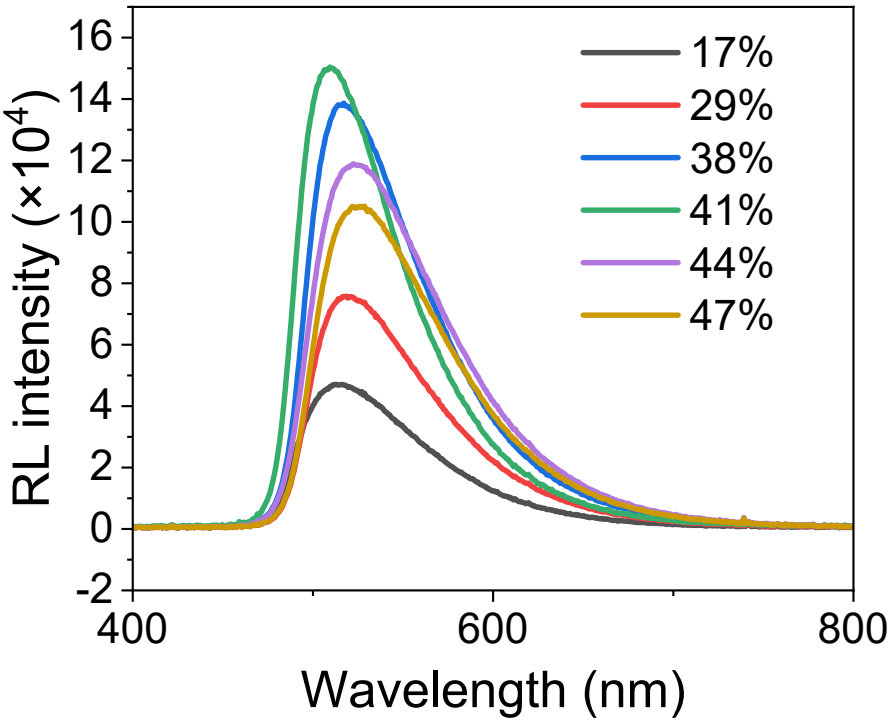

Figure S11 0.1 mm thickness PMMA doped films of I-CzBN: from 17% to 47%. Dose rate: 212.97 μGy s^{-1}.

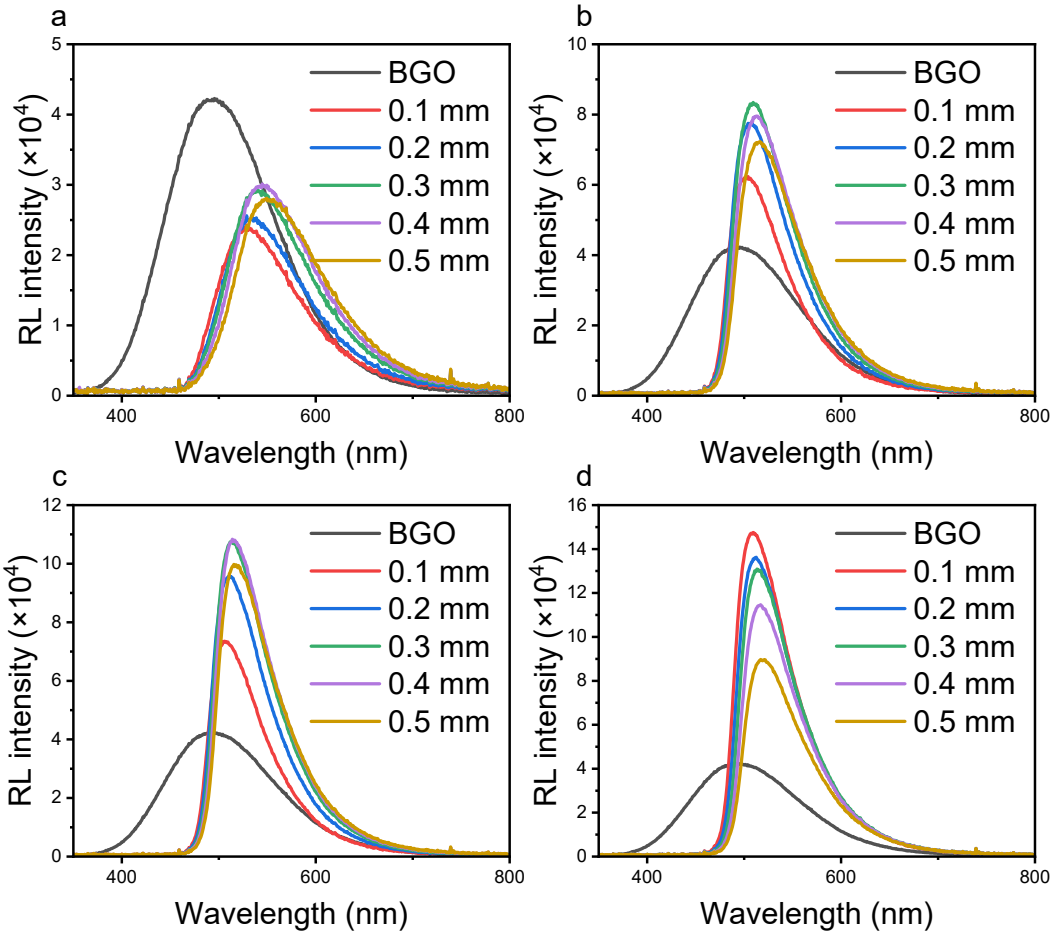

Figure S12 Radioluminescence spectra of the (a) H-CzBN, (b) Cl-CzBN, (c) Br-CzBN, and (d) I-CzBN with 41 wt% doped in PMMA matrix at different thicknesses compared to the reference scintillator, BGO. Dose rate：212.97 μGy s^{-1}.

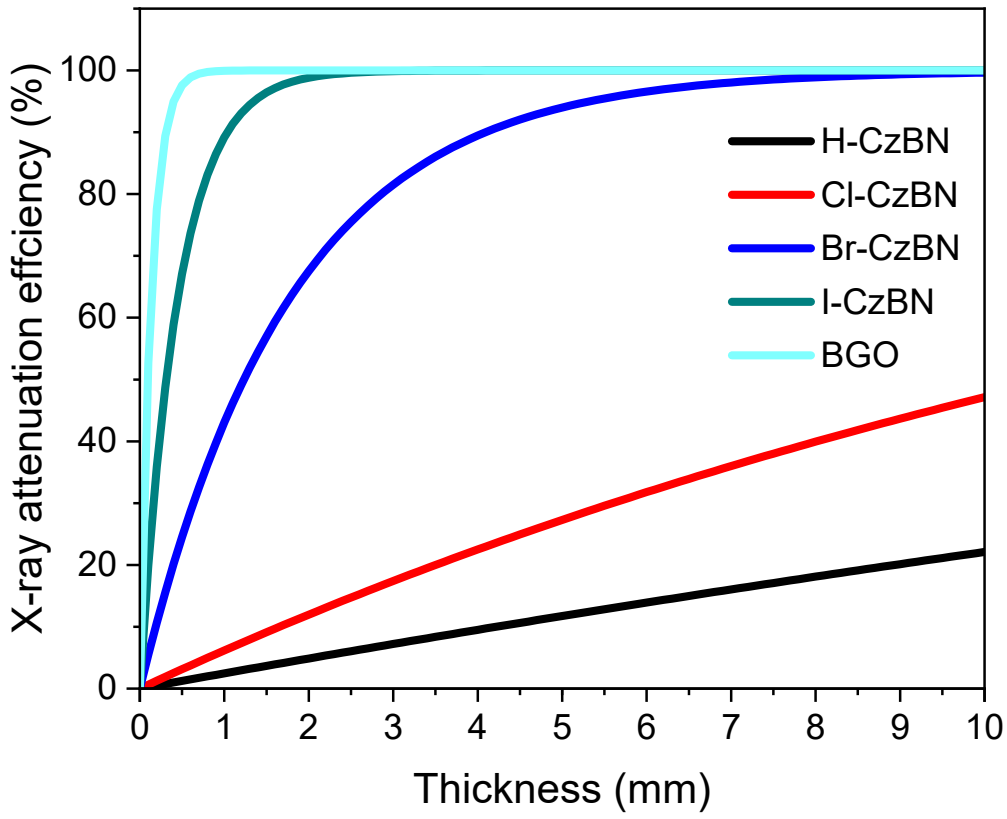

Figure S13 Calculated X-ray attenuation efficiencies of H-CzBN, Cl-CzBN, Br-CzBN, I-CzBN and BGO versus thicknesses of these scintillators.

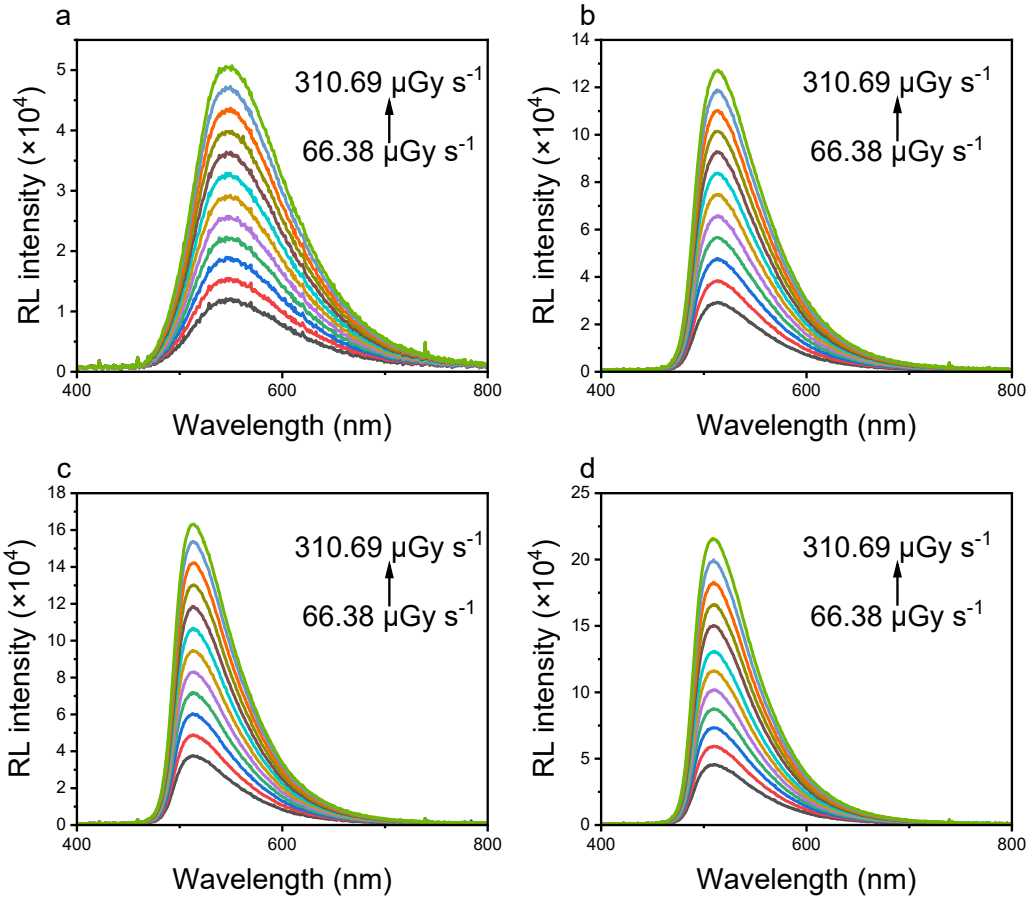

Figure S14 Dosage dependent radioluminescence intensity in the range of 66.38 to 310.69 μGy s^{-1} of (a) H-CzBN, (b) Cl-CzBN, (c) Br-CzBN, (d) I-CzBN.

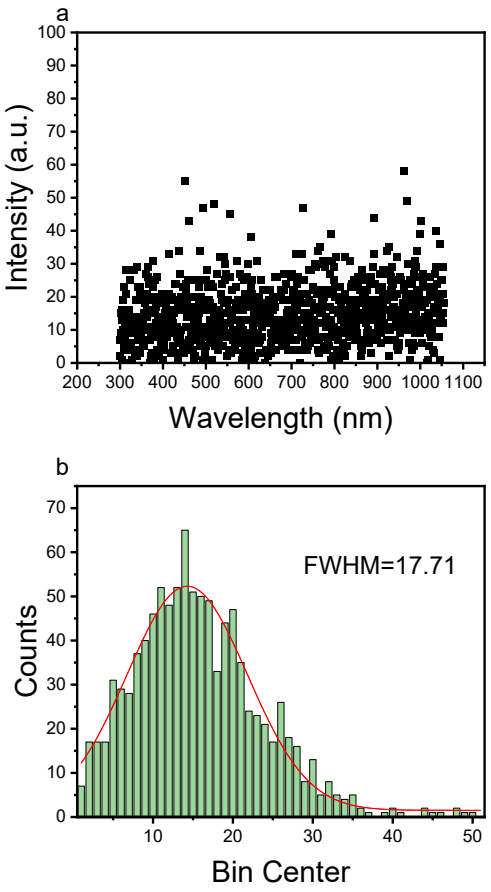

Figure S15 Background measurements. (a) The background signal of the radioluminescence spectra. (b) Background signal fitted with Gaussian function (Full width at half maximum: FWHM = 17.71).

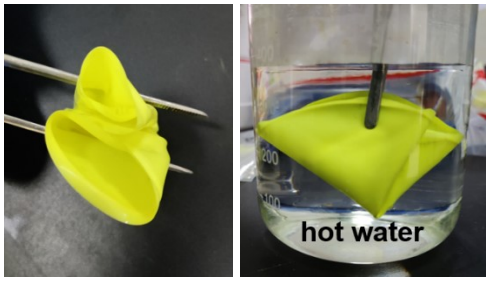

Figure S16 The flexible PDMS film under daylight (left) and hot water (right).

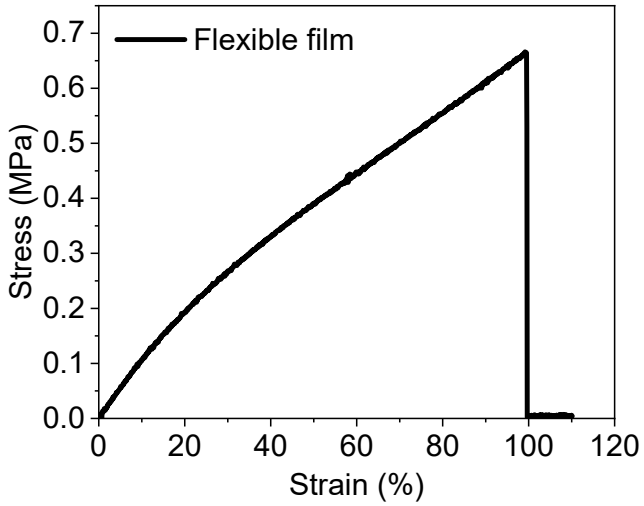

Figure S17 The stretchability of the flexible PDMS film.

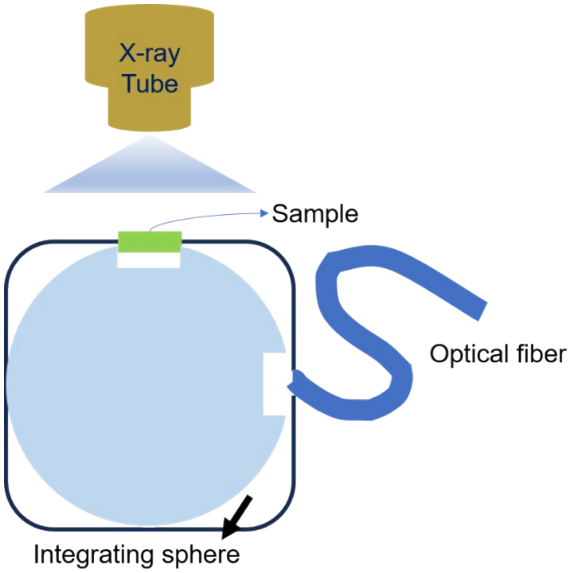

Figure S18 Schematic of the testing system for radioluminescence (RL) intensity measurement.

Table S1 Calculated S_1, T_1 and ΔE_{ST} of R-CZBN in neat film.

	S_1 (eV)	T_1 (eV)	ΔE_{ST} (eV)
H-CzBN	2.68	2.54	0.14
Cl-CzBN	2.66	2.61	0.05
Br-CzBN	2.71	2.63	0.08
I-CzBN	2.62	2.61	0.01

Table S2 Photophysical properties of R-CzBN in degassed toluene.

	τ_p (ns)	τ_d (μs)	Φ_p	Φ_d	k_p (10^7 s^{-1})	k_d (10^5 s^{-1})	k_{ISC} (10^7 s^{-1})	k_{RISC} (10^6 s^{-1})
H-CzBN	12	4.9	0.276	0.524	2.3	1.1	1.7	0.29
Cl-CzBN	8.0	2.9	0.236	0.714	2.95	2.5	2.3	0.99
Br-CzBN	1.3	1.0	0.09	0.81	6.92	8.1	6.3	8.01
I-CzBN	0.8	0.37	0.114	0.636	14.25	17.2	12.6	10.8

Table S3 PLQYs, relative light yields and detection limits of four TADF chromophores doped in PMMA matrix with 41 wt%.

Samples	PLQYs (%)	Relative light yields (photons MeV^{-1})	Detections limits (nGy^{-1})
H-CzBN	50	6228	332.5
Cl-CzBN	56	11846	131.3
Br-CzBN	53	14457	101.2
I-CzBN	40	19306	75.4

Table S4 The Spatial Resolution of some typical TADF organic scintillators and I-CzBN in this work.

Scintillator	**Spatial Resolution (lp mm^{-1})**	**Reference**
DMAC-TRZ	16.6	1
TADF-Br	>18.0	3
BMAT	20.0	4
TADF-Br & Ir-OMC	19.8	5
TADF-Br & Rubene	27.5	6
4CzIPN-I & 4CzTPN	20	7
C4-I	>14.0	8
I-CzBN	>20	This work

Table S5 The relationship between voltage, current, and corresponding dose rate X-ray used for the experiments.

Voltage (kV)	Current (μA)	Dose rate (μGy s^{-1})
40	60	66.4
	80	88.6
	100	110.8
	120	132.8
	140	155.0
	160	177.2
	180	199.4
	200	221.4
	220	243.6
	240	265.8
	260	288.0
	280	310.2

References

[1] J.X. Wang, L. Gutiérrez-Arzaluz, X. Wang et al, Heavy-Atom Engineering of Thermally Activated Delayed Fluorophores for High-Performance X-Ray Imaging Scintillators, *Nat. Photonics* 2022 **16** 869.

[2] Gaussian 16, Revision A.03,

M. J. Frisch, G. W. Trucks, H. B. Schlegel, G. E. Scuseria, M. A. Robb, J. R. Cheeseman, G. Scalmani, V. Barone, G. A. Petersson, H. Nakatsuji, X. Li, M. Caricato, A. V. Marenich, J. Bloino, B. G. Janesko, R. Gomperts, B. Mennucci, H. P. Hratchian, J. V. Ortiz, A. F. Izmaylov, J. L. Sonnenberg, D. Williams-Young, F. Ding, F. Lipparini, F. Egidi, J. Goings, B. Peng, A. Petrone, T. Henderson, D. Ranasinghe, V. G. Zakrzewski, J. Gao, N. Rega, G. Zheng, W. Liang, M. Hada, M. Ehara, K. Toyota, R. Fukuda, J. Hasegawa, M. Ishida, T. Nakajima, Y. Honda, O. Kitao, H. Nakai, T. Vreven, K. Throssell, J. A. Montgomery, Jr., J. E. Peralta, F. Ogliaro, M. J. Bearpark, J. J. Heyd, E. N. Brothers, K. N. Kudin, V. N. Staroverov, T. A. Keith, R. Kobayashi, J. Normand,

K. Raghavachari, A. P. Rendell, J. C. Burant, S. S. Iyengar, J. Tomasi, M. Cossi, J. M. Millam, M. Klene, C. Adamo, R. Cammi, J. W. Ochterski, R. L. Martin, K. Morokuma, O. Farkas,

J. B. Foresman, and D. J. Fox, Gaussian, Inc., Wallingford CT, 2016.

[3] W. Ma, Y. Su, Q. Zhang, C. Deng, L. Pasquali, W. Zhu, Y. Tian, P. Ran, Z. Chen, G. Yang, G. Liang, T. Liu, H. Zhu, P. Huang, H. Zhong, K. Wang, S. Peng, J. Xia, H. Liu, X. Liu and Y. M. Yang, Thermally activated delayed fluorescence (TADF) organic molecules for efficient X-ray scintillation and imaging, *Nat. Mater.*, 2022, **21**, 210-216.

[4] J.-X. Wang, L. Gutiérrez-Arzaluz, X. Wang, T. He, Y. Zhang, M. Eddaoudi, O. M. Bakr and O. F. Mohammed, Heavy-atom engineering of thermally activated delayed fluorophores for high-performance X-ray imaging scintillators, *Nat. Photonics*, 2022, **16**, 869-875.

[5] X. Wang, G. Niu, Z. Zhou, Z. Song, K. Qin, X. Yao, Z. Yang, X. Wang, H. Wang, Z. Liu, C. Yin, H. Ma, K. Shen, H. Shi, J. Yin, Q. Chen, Z. An and W. Huang,

Halogenated Thermally Activated Delayed Fluorescence Materials for Efficient Scintillation, *Research*, 2023, **6**, 0090.

[6] J.-X. Wang, I. Dutta, J. Yin, T. He, L. Gutiérrez-Arzaluz, O. M. Bakr, M. Eddaoudi, K.-W. Huang and O. F. Mohammed, Triplet-triplet energy-transfer-based transparent X-ray imaging scintillators, *Matter*, 2023, **6**, 217-225.

[7] J.-X. Wang, J. Yin, L. Gutiérrez-Arzaluz, S. Thomas, W. Shao, H. N. Alshareef, M. Eddaoudi, O. M. Bakr and O. F. Mohammed, Singlet Fission-Based High-Resolution X-Ray Imaging Scintillation Screens, *Adv. Sci.*, 2023, **10**, 2300406.

[8] S. A. Alomar, J.-X. Wang, L. Gutiérrez-Arzaluz, S. Thomas, H. N. Alshareef, O. M. Bakr, M. Eddaoudi and O. F. Mohammed, TADF-Based X-ray Screens with Simultaneously Efficient Singlet and Triplet Energy Transfer for High Spatial Imaging Resolution, *ACS Appl. Mater. Interfaces*, 2023, **15**, 34263-34271.

[9] J.-H. Wei, J.-B. Luo, Z.-L. He, Q.-P. Peng, J.-H. Chen, Z.-Z. Zhang, X.-X. Guo and D.-B. Kuang, Phosphonium Iodide Featuring Blue Thermally Activated Delayed Fluorescence for Highly Efficient X-Ray Scintillator, *Angew. Chem. Int. Ed.*, 2024, **63**, e202410514.